Supporting Information

Munro et al. 10.1073/pnas.1205396109

SI Text

Derivation of Eqs. 7 and 8. We show here how Eqs. **7** and **8** are derived. We begin by defining a quantity I_P as

$$I_P(\Delta P) = \int_{-\infty}^{\infty} K(x, \Delta P)|U_0(x)|^2 dx \qquad \textbf{[S1]}$$

such that $I_L = I_P(-P/2)$ and $I_R = I_P(P/2)$. Substituting Eq. **2** into Eq. **S1** an introducing $f(\xi_i) = \exp(-k\mu(\xi_i))$, we obtain

$$I_P(\Delta P) = \int_{-\infty}^{\infty} K(x, \Delta P)\left|\sum_i \sqrt{\frac{2\pi}{k|g''(\xi_i, x)|}} f(\xi_i) \times \exp\left(i\left[kg(\xi_i, x) + \frac{\pi}{4}\mathrm{sgn}(g''(\xi_i, x))\right]\right)\right|^2 dx. \qquad \textbf{[S2]}$$

Note that for clarity, in this section we write ξ_i instead of $\xi_i(x)$. Following the definition of Eq. **6**, repeated here for clarity

$$h:\ [-W/2, W/2] \to \mathbb{R} \qquad \xi \mapsto z_{\mathrm{od}}\phi'(\xi) + M\xi,$$

we introduce a partition $\Omega = [-W/2, W/2] = \cup_i \Omega_i$ and h_i such that each h_i is injective:

$$h_i:\ \Omega_i \to \mathbb{R} \qquad \xi \mapsto h(\xi) \qquad \textbf{[S3]}$$

finally allowing us to define p_i as

$$p_i:\ h(\Omega_i) \to \Omega_i \qquad x \mapsto h_i^{-1}(x). \qquad \textbf{[S4]}$$

For brevity we introduce

$$a(\xi_i, x) = f(\xi_i)\exp\left(i\left[kg(\xi_i, x) + \frac{\pi}{4}\mathrm{sgn}(g''(\xi_i, x))\right]\right), \qquad \textbf{[S5]}$$

which enables us to write Eq. **S2** as

$$\begin{aligned}
I_P(\Delta P) &= \int_{-\infty}^{\infty} K(x, \Delta P)\left|\sum_i \sqrt{\frac{2\pi}{k|g''(\xi_i, x)|}} a(\xi_i, x)\right|^2 \mathrm{d}x \\
&= \int_{-\infty}^{\infty} K(x, \Delta P)\left(\sum_i \sqrt{\frac{2\pi}{k|g''(\xi_i, x)|}} a(\xi_i, x)\right)\left(\sum_j \sqrt{\frac{2\pi}{k|g''(\xi_j, x)|}} a^*(\xi_j, x)\right)\mathrm{d}x \\
&= \int_{-\infty}^{\infty} K(x, \Delta P)\left(\sum_i \frac{\lambda}{|g''(\xi_i, x)|}|a(\xi_i, x)|^2 + \sum_i \sum_{j\neq i} \frac{\lambda}{\sqrt{|g''(\xi_i, x)||g''(\xi_j, x)}}\right)\mathrm{d}x \\
&= \sum_i \int_{h(\Omega_i)} K(x, \Delta P)\frac{\lambda}{|g''(p_i(x), x)|}|a(p_i(x), x)|^2 \mathrm{d}x \\
&+ 2\Re\sum_i \sum_{j>i} \frac{\lambda}{\sqrt{|g''(p_i(x), x)g''(p_j(x), x)|}} \int_{h(\Omega_i)\cap h(\Omega_j)} K(x, \Delta P)a(p_i(x), x)\overline{a(p_j(x), x)}\mathrm{d}x,
\end{aligned} \qquad \textbf{[S6]}$$

where * represents complex conjugation and $\Re$ the real part of a complex valued quantity. Up until now the summation indices depend upon the value of x and, in particular, which $h(\Omega_i)$ it is a member of. We now change the variable of integration according to $x = h(\xi)$. Noting that $\mathrm{d}x = h'(\xi)d\xi$ and that $h'(\xi) = z_{\mathrm{od}}g''(\xi)$ we can write Eq. **S6** as

$$\begin{aligned}
I_P(\Delta P) &= \sum_i \int_{\Omega_i} K(h(\xi), \Delta P)\lambda z_{\mathrm{od}}|a(\xi, h(\xi))|^2 \mathrm{d}\xi \\
&+ \sum_i \sum_{j>i} \int_{h_i^{-1}(h(\Omega_i)\cap h(\Omega_j))} K(h(\xi), \Delta P)\lambda z_{\mathrm{od}}\sqrt{\frac{|g''(\xi, h(\xi))|}{|g''(\xi_j, h(\xi))|}} 2\Re\{a(\xi, h(\xi))\overline{a(\xi_j, h(\xi))}\}\mathrm{d}\xi \\
&= \int_{\Omega} K(h(\xi), \Delta P)\lambda z_{\mathrm{od}}|a(\xi, h(\xi))|^2 \mathrm{d}\xi \\
&+ \sum_i \sum_{j>i} \int_{h_i^{-1}(h(\Omega_i)\cap h(\Omega_j))} K(h(\xi), \Delta P)\lambda z_{\mathrm{od}}\sqrt{\frac{|g''(\xi, h(\xi))|}{|g''(\xi_j, h(\xi))|}} 2\Re\{a(\xi, h(\xi))\overline{a(\xi_j, h(\xi))}\}\mathrm{d}\xi \\
&= \int_{\Omega} K(h(\xi), \Delta P)\lambda z_{\mathrm{od}} f^2(\xi)\mathrm{d}\xi \\
&+ \sum_i \sum_{j>i} \lambda z_{\mathrm{od}} \int_{h_i^{-1}(h(\Omega_i)\cap h(\Omega_j))} 2K(h(\xi), \Delta P)f(\xi)f(\xi_j)\sqrt{\frac{|g''(\xi, h(\xi))|}{|g''(\xi_j, h(\xi))|}} \\
&\cdot \left(\begin{cases} \cos(k(g(\xi) - g(\xi_j))), & \mathrm{sgn}(g''(\xi, h(\xi))) = \mathrm{sgn}(g''(\xi_j, h(\xi))) \\ -\mathrm{sgn}(g''(\xi, h(\xi)))\sin(k(g(\xi) - g(\xi_j))), & \text{otherwise} \end{cases}\right) \cdot \mathrm{d}\xi.
\end{aligned} \qquad \textbf{[S7]}$$

In the polychromatic case for which we are principally interested, the second term in Eq. **S7** tends to zero due to the rapid oscillation of the integral kernel as k varies. This is a result of the loss of visibility observed in any interference experiment when polychromatic light is employed. In the monochromatic case it is necessary to assume that the object completely covers the open region of aperture A_1. Then, following Gureyev and Wilkins (1), by making the assumption that

$$|\partial_\xi^m \phi(\xi)| \ll (Z')^{1-m}, \qquad m^2 > 0, \qquad \textbf{[S8]}$$

where $Z' = z_{so} z_{od}/(z_{so} + z_{od})$, $g'(\xi, x)$ will have at most one solution for each value of x, which removes the second term in Eq. **S7**. Upon substituting back $f(\xi) = \exp(-k\mu(\xi))$ into Eq. **S7** we obtain

$$I_P(\Delta P) = \lambda z_{od} \int_\Omega K(h(\xi), \Delta P) \exp(-2k\mu(\xi)) d\xi$$

from which Eqs. **7** and **8** are directly obtained.

Discussion on a Possibly Erroneous Phase Gradient. Observation of Eq. **13** reveals that it is possible for a sample possessing only an absorption gradient to generate a possibly erroneous phase gradient. This would occur if a difference between I_R and I_L was produced by an absorption gradient. Such an erroneous phase gradient is, however, made practically negligible by using an incoherent source because the extended source acts to average the absorption gradient over a single aperture. Further, in the case of a point source, we have developed a method for correcting for this erroneous phase gradient. Because this paper is focused on incoherent sources we first give an example that demonstrates how using an incoherent source mitigates this problem. We then derive the method for correcting for an erroneous phase gradient.

To demonstrate how using an incoherent source mitigates the problem of erroneous phase gradient, we have performed some simulations for a wedge-like object composed of sapphire, using a rigorous model outlined in detail in previous publications (2, 3). We made two approximations in performing this simulation because we do not need to make comparisons with experiment as part of this test. The first approximation is the spectrum because it is difficult to measure the spectrum of our source because of the intense flux. We thus employed a simulation by Boone et al. (4) that assumes a source geometry partly different to that of the Rigaku 007HF. The simulated spectrum is plotted in Fig. S1. The second approximation is that we modelled δ and β for sapphire with the relationship

$$\delta(E) = \delta_{E_{ref}} \left(\frac{E_{ref}}{E}\right)^2, \qquad \textbf{[S9]}$$

$$\beta(E) = \beta_{E_{ref}} \left(\frac{E_{ref}}{E}\right)^4, \qquad \textbf{[S10]}$$

where $E_{ref} = 20$ kV is a reference photon energy and $\delta_{E_{ref}} = 2.03 \times 10^{-6}$ and $\beta_{E_{ref}} = 3.99 \times 10^{-9}$ are, respectively, the values of δ and β at the reference energy (5). This approximation means that the simulated results might differ slightly from that measured experimentally as it neglects absorption edges. However, it is adequate because we wish only to demonstrate a trend for typical materials.

The simulation then progressed by simulating the XPCI image for both setups in Fig. 1 for the configuration used to image the ground beetle. The sample was a wedge-like object as depicted in Fig. 1 with a thickness at the centre of 200 μm. Four different slopes (1, 2, 3, and 4) were considered for a range of source sizes between an ideal point source to source FWHM of 100 μm. Two simulations were performed in each case, one with the correct distribution of $\delta(E)$ and one with $\delta(E) = 0$. The erroneous phase gradient error was then defined as

$$\epsilon_{\bar{\phi}'} = \frac{\bar{\phi}'|^{\delta(E)=0}}{\bar{\phi}'|^{\delta(E)=\delta_{E_{ref}}(\frac{E_{ref}}{E})^2}}. \qquad \textbf{[S11]}$$

The erroneous phase gradient is plotted for a range of source FWHM in Fig. S2, which shows that the erroneous error reduces as the source FWHM increases. In all of our experiments where an incoherent source has been used the erroneous phase gradient has been an insignificant source of error.

Even though the subject of this paper is incoherent sources we would like to point out that it is possible to rigorously correct for the erroneous phase gradient when a point source is used. We present the mathematical analysis of this technique here. Instead of assuming that μ is constant within a single open region of the presample aperture we allow it to vary linearly. Because we consider the geometry in Fig. 1, without loss of generality, we expand both ϕ and μ in Taylor series about $\xi = 0$ as

$$\phi(\xi) = \phi(0) + \left.\frac{\partial \phi}{\partial \xi}\right|_0 (\xi - \xi_s), \qquad \textbf{[S12]}$$

$$\mu(\xi) = \mu(0) + \left.\frac{\partial \mu}{\partial \xi}\right|_0 (\xi - \xi_s), \qquad \textbf{[S13]}$$

where we have included the parameter ξ_s to allow subpixel scanning of the sample to be modelled. Upon substituting both of these expressions into Eq. **13** for the case of a point source, direct evaluation without approximation yields

$$I_R - I_L = \frac{C \exp(-2k\mu(0)) \exp(2k\partial\mu/\partial\xi|_0 \xi_s)}{k\partial\mu/\partial\xi|_0} \cdot [\cosh(k\partial\mu/\partial\xi|_0 W) - \exp(2k\partial\mu/\partial\xi|_0 z_{od}\phi'/M)] \qquad \textbf{[S14]}$$

$$I_R + I_L = \frac{C \exp(-2k\mu(0)) \exp(2k\partial\mu/\partial\xi|_0 \xi_s)}{k\partial\mu/\partial\xi|_0} \sinh(k\partial\mu/\partial\xi|_0 W) \qquad \textbf{[S15]}$$

$$\frac{I_R - I_L}{I_R + I_L} = \frac{\exp(2k\partial\mu/\partial\xi|_0 z_{od}\phi'/M) - \cosh(k\partial\mu/\partial\xi|_0 W)}{\sinh(k\partial\mu/\partial\xi|_0 W)}, \qquad \textbf{[S16]}$$

where $\cosh(k\partial\mu/\partial\xi|_0 W)$ leads to the potentially erroneous phase gradient. Suppose now that measurements are taken for scanning steps $\xi_s = -\Delta\xi, 0, \Delta\xi$ where $\Delta\xi$ is a subpixel quantity.

For example, in the ground beetle and phantom images, $\Delta\xi$ was approximately 8 μm,which is calculated by dividing the pitch of A_1 by the number of subpixel scanning positions used to acquire the image. Then $\partial\mu/\partial\xi|_0$ may be extracted as

$$k\left.\frac{\partial \mu}{\partial \xi}\right|_0 = \frac{1}{4\Delta\xi} \log\left[\frac{(I_R + I_L)|^{\xi_s=\Delta\xi}}{(I_R + I_L)|^{\xi_s=-\Delta\xi}}\right], \qquad \textbf{[S17]}$$

which allows $k\partial\mu/\partial\xi|_0 W$ to be calculated. In the case of a large phase gradient, unlikely to be encountered in practice, Eq. **S16** may be inverted without approximation as

$$\phi' = \log\left[\left.\frac{I_R - I_L}{I_R + I_L}\right|^{\xi_s=0} \sinh(k\partial\mu/\partial\xi|_0 W) + \cosh(k\partial\mu/\partial\xi|_0 W)\right] \frac{M}{2kz_{od}\partial\mu/\partial\xi}, \qquad \textbf{[S18]}$$

however, by substituting $\log(1+x) \approx x$, $\sinh(x) \approx x$, and $\cosh(x) \approx 1 + x^2/2$ for small x, we obtain

$$\phi' = \left[\frac{I_R - I_L}{I_R + I_L}\right|^{\xi_s=0} + \frac{1}{2} k\partial\mu/\partial\xi|_0 W \Bigg] \frac{P}{2z_{\text{od}}}. \qquad \textbf{[S19]}$$

Eqs. **S18** and **S19** thus show that the erroneous phase gradient may be corrected because Eq. **S17** allows $k\partial\mu/\partial\xi|_0 W$ to be calculated. This means that whereas only two images are required to perform quantitative XPCI with an extended source, more images may be required if a point source is used in the presence of strong absorption gradients.

Further Explanation of Fig. 2 *C* and *D*. An interesting question that arises from Fig. 2 is why the positive peaks in the titanium raw profiles are nulled to form the absorption image. Although this must be the case due to energy conservation it is accommodated in the raw profiles due to an asymmetry that can be observed in the magnified plots of the titanium profiles from Fig. 2 as shown in Fig. S3. These raw profiles, normalized only by the equivalent profile in the absence of a sample (i.e., "flat fielded"), show that the profiles are in fact offset by a subpixel amount. Further, they also show a change in the slope of the profile where the negative peak would be in less absorbing samples. This is indicated by the arrow associated with configuration I_R in Fig. S3. The physical reason for this is explained by noting the two distinct imaging regimes that are responsible for the profiles in Fig. S3. The first and perhaps most general regime is that depicted in the I_R configuration of Fig. S3 in which the system is sensitive to both sample absorption and phase gradients. In this case, when imaging a low-absorbing sample, a negative peak would be observed if photons originally incident upon the open region of A_2 are refracted into the absorbing region of A_2. In the case of a highly absorbing sample such as titanium, the reduction in photons due to refraction is less than the maximum reduction observed due to absorption in the sample. Thus a negative peak is not produced. In the alternate regime depicted in the I_L configuration a positive peak results because photons originally incident upon the absorbing region of A_2 are refracted into the open region thus producing a signal greater than that when no sample is present. The asymmetry arises essentially because the profile minimum can be determined by absorption or refraction whereas the peak is determined by refraction only. It should be noted that we include titanium as the pathological case because nowhere have we seen phase and absorption retrieval techniques demonstrated for such highly absorbing samples.

1. Gureyev T, Wilkins S (1998) On x-ray phase imaging with a point source. *J Opt Soc Am A* 15:579–585.
2. Munro PRT, Ignatyev K, Speller RD, Olivo A (2010) The relationship between wave and geometrical optics models of coded aperture type X-ray phase contrast imaging systems. *Opt Express* 18:4103–4117.
3. Munro PRT, Ignatyev K, Speller RD, Olivo A (2010) Source size and temporal coherence requirements of coded aperture type X-ray phase contrast imaging systems. *Opt Express* 18:19681–19692.
4. Boone J, Fewell T, Jennings R (1997) Molybdenum, rhodium, and tungsten anode spectral models using interpolating polynomials with application to mammography. *Med Phys* 24:1863–1874.
5. Henke BL, et al. (1993) X-ray interactions: Photoabsorption, scattering, transmission, and reflection at E = 50–30,000 eV, Z = 1-92. *Atom Data Nucl Data* 54:181–342.

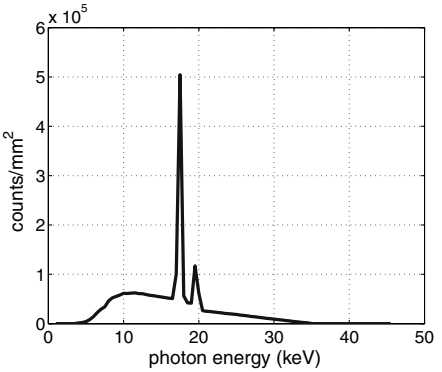

Fig. S1. Plot of photon fluence from an X-ray source with a Mo target and a tube voltage of 35 kV (1).

1 Boone J, Fewell T, Jennings R (1997) Molybdenum, rhodium, and tungsten anode spectral models using interpolating polynomials with application to mammography. *Med Phys* 24:1863–1874.

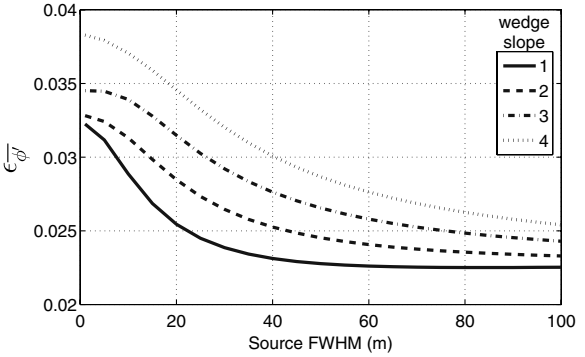

Fig. S2. Plots of erroneous phase gradient as a proportion of the actual phase gradient for a range of source FWHM.

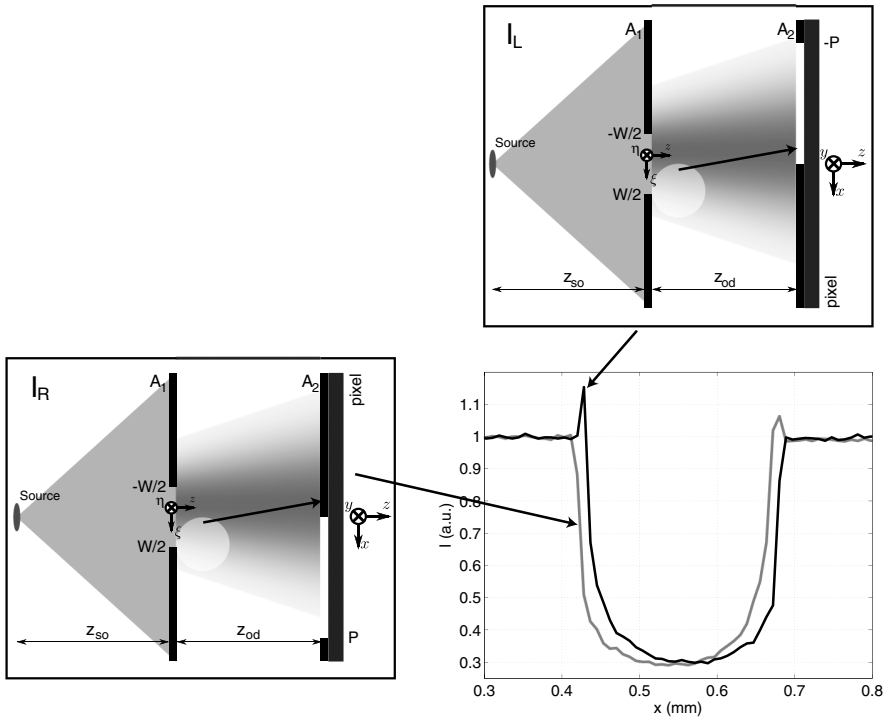

Fig. S3. Magnified plots of I_L and I_R from Fig. 2*C* as well as the image and sample configurations (not to scale) that produced the positive and negative peaks.